# Magnetic-field effects on one- and two-hole states in parabolic quantum dots

F. B. Pedersen
*Institutt for Fysikk, Norges Teknisk-Naturvitenskapelige Universitet, N-7034 Trondheim, Norway*

Yia-Chung Chang
*Department of Physics and Materials Research Laboratory, University of Illinois at Urbana-Champaign, Urbana, Illinois 61801*
(Received 27 September 1996)

Using a multiband effective-mass theory, we have calculated the one- and two-hole energies in a parabolic quantum dot in the presence of a perpendicular magnetic field. The valence-band degeneracy, the Coulomb interaction, and the effect of finite offsets are all taken into account. The energies are calculated variationally with an iterative relaxation technique. The single-hole levels show strong anticrossings due to the valence-band mixing. As a result they have in general a weaker field dependence compared with the corresponding uncoupled levels. For the two-hole states both the valence-band mixing and the Coulomb interaction are shown to be substantial. The correlations between the holes are strong enough to change the total angular momentum of the ground state when the magnetic field is increased. [S0163-1829(97)10907-9]

## I. INTRODUCTION

Modern lithographic techniques have made possible the fabrication of individual quantum dots.[1] Such structures confine electrons (or holes) in all three spatial dimensions and thus have a fully quantized energy spectrum. Usually their width in the growth direction is much smaller than their lateral extensions, so these quantum dots may be regarded as artificial atoms with disklike shapes. By varying the applied gate potential over the dot, the number $N$ ($N=0,1,2,3,...$) of electrons can be controlled; increasing the gate potential it is possible to charge the dot with an additional *single* electron. Recently Ashoori *et al.* used single-electron capacitance spectroscopy (SECS) to study the $N$-electron ground state of such isolated quantum dots in a magnetic field, thus measuring the ground state of different ''quantum-dot elements.''[2] Their experimental results for the low-lying levels were well described in terms of a lateral confinement potential that was parabolic. Other studies, both experimental[3] and theoretical,[4,5] also support the view that in these dots the lateral confinement potential can be approximated by a (one-parameter adjustable) parabolic potential.

Few-electron systems in quantum dots have been extensively studied, both with and without an applied magnetic field.[4–15] For the dots in question the electron-electron interaction, the confinement energy, the Zeeman energy, and the cyclotron energy are all on the meV scale, and must consequently be treated on an equal footing. Most studies have therefore employed a full numerical solution, although special cases exist where an analytical approach is possible. Taut[9] has recently found exact solutions of the two-electron problem for certain values of the confinement potential. El-Said[13] has studied the same problem perturbatively using the shifted $1/D$ expansion ($D$ is spatial dimensionality), while Johnson and co-workers[10,11] solved the $N$-electron problem exactly for $r^2$ and $1/r^2$ electron-electron interactions.

The ground states in such quantum dots exhibit interesting properties. For the two-electron case Wagner, Merkt, and Chaplik[7] found that the ground-state angular momentum increases with the applied magnetic field in order to minimize the Coulomb repulsion. Concomitant spin-singlet–spin-triplet transitions resulted. In the high-field limit the singlet case is suppressed by the Zeeman effect, and only triplet-triplet transitions occur. Maksym and Chakraborty[8] studied this spin-polarized limit for an arbitrary number of electrons and found that only certain ''magic values'' of the total angular momentum occurred for the ground state. These incompressible ground states are believed to be reminiscent of a fractional quantum Hall system. In view of the exotic effects present in few-electron systems, the far-infrared (FIR) absorption spectrum of parabolic quantum dots was surprisingly simple, being dominated by peaks at the single-electron energies and essentially independent of the number of electrons on the dot as well as the specific form of the electron-electron interaction. This is no paradox however, merely a manifestation of the generalized Kohn's theorem:[6,8,17–20] The parabolic confinement potential allows for a separation of the problem into a center-of-mass (CM) and a relative part, and the dipole operator only couples to the CM part. Since the CM spectrum is identical to the single-particle spectrum, one sees only features at the single-electron energies. It is not difficult, however, to find situations where Kohn's theorem is violated. Deviations from a strict parabolic confinement potential will result in additional resonances in FIR experiments.[14,15] The same is true for quantum dots prepared as nanocrystallites, as they typically have a hard-wall confinement potential that mixes the relative and CM motion.[16]

In this work we study hole states in a GaAs quantum dot in the presence of a magnetic field. The dot is made from a $GaAs/Al_{0.3}Ga_{0.7}As$ [001] quantum-well material. Although the lateral confinement potential is taken to be parabolic, the strong mixing between the valence bands makes Kohn's theorem invalid for hole states.[21–23] It is therefore essential to make use of a multiband effective-mass theory in this case. Using an axial approximation for the 4 degenerate $\Gamma_8$ states in GaAs we calculate variationally the low-lying energy levels for single-hole and two-hole states as a function

 

of the magnetic field. The effect of the finite quantum-well potential is accounted for in an approximate manner. Our results for the single-hole levels agree well with the calculations of Broido, Cros, and Rössler.[22] The coupling of the various bands by the off-diagonal terms in the Luttinger Hamiltonian leads to anticrossings in the energy spectrum, giving in general a weaker field dependence compared with the uncoupled (electronic) case. The results from the two-hole calculations show that both the off-diagonal coupling terms and the Coulomb interaction contribute substantially to the two-hole energy. Neither effect should therefore be neglected in realistic calculations. Moreover, the Coulomb interaction induces strong correlations between the holes. As a result the symmetry of the ground state is changed with increasing magnetic field.

In Sec. II we present the model and the basis functions used in the variational calculation. Section III contains the numerical results along with a discussion. A short summary is given in Sec. IV.

## II. GENERAL THEORY

This section is divided into two subsections. In the first subsection we present the model used. Then we construct appropriate basis states for the single-hole and two-hole problem. As much of the theory from the field-free case still applies, we omit some of the details. The interested reader is referred to Ref. 24 for a more thorough discussion.

### A. Model

In bulk GaAs the topmost valence bands consist of the 4 $\Gamma_8$ states, which are degenerate at $\mathbf{k}=0$. They are separated by an energy 1.5 eV from the conduction band and by 0.35 eV from the split-off band at $\mathbf{k}=0$. We are only interested in energies less than, say, 100 meV, and it is therefore sufficient only to take the $\Gamma_8$ states into account. In this strong spin-orbit situation the $\Gamma_8$ quadruplet corresponds to the $J=3/2$, $j_z=\pm 1/2, \pm 3/2$ states.

In the effective-mass approximation the kinetic energy of the hole is described by the Luttinger Hamiltonian[25]

$$H_L=\frac{\hbar^2}{2m_0}\begin{bmatrix} H_h & R & S & 0 \\ R^* & H_l & 0 & S \\ S^* & 0 & H_l & -R \\ 0 & S^* & -R^* & H_h \end{bmatrix}, \tag{1}$$

where

$$\begin{aligned} H_h&=(\gamma_1+\gamma_2)(k_x^2+k_y^2)+(\gamma_1-2\gamma_2)k_z^2, \\ H_l&=(\gamma_1-\gamma_2)(k_x^2+k_y^2)+(\gamma_1+2\gamma_2)k_z^2, \\ R&=2\sqrt{3}\,\gamma_3 i k_- k_z, \\ S&=\sqrt{3}\,\gamma k_-^2, \end{aligned} \tag{2}$$

and

$$\begin{aligned} \mathbf{k}&=-i\nabla-e\mathbf{A}/\hbar, \\ k_\pm&=k_x\pm ik_y. \end{aligned} \tag{3}$$

Here $\gamma_1, \gamma_2$, and $\gamma_3$ are the Luttinger parameters, $\gamma=1/2(\gamma_2+\gamma_3)$, and $m_0$ is the free-electron mass. We have adopted the axial approximation and the Hamiltonian is represented in the hole picture, where the sign of the energy is reversed. **A** is the vector potential, which in the symmetric gauge reads

$$\mathbf{A}=\mathbf{B}\times\mathbf{r}/2=(-y,x)B/2 \tag{4}$$

for a magnetic field in the $z$ direction. The quantum-well potential in the growth direction is accounted for by a finite potential well of width $w$

$$V_\perp(z)=\begin{cases} \Delta E_v & \text{for } |z|\geq w/2, \\ 0 & \text{for } |z|<w/2. \end{cases} \tag{5}$$

The lateral confinement potential is parabolic, viz.,

$$V_\parallel(\boldsymbol{\rho})=\frac{1}{2}K\rho^2 \tag{6}$$

in cylindrical coordinates. The constant $K$ measures the strength of the potential. We will also describe the parabolic potential in terms of its characteristic frequency $\omega_0=\sqrt{K/m_h}$ and its characteristic length $l_0=\sqrt{\hbar/m_h\omega_0}$. Both of these quantities are defined in terms of the (in-plane) heavy-hole mass $m_h=m_0/(\gamma_1+\gamma_2)$. The hole-hole interaction is modeled by a statically screened Coulomb potential:

$$V(\mathbf{r}_1,\mathbf{r}_2)=\frac{e^2}{4\pi\epsilon|\mathbf{r}_2-\mathbf{r}_1|}. \tag{7}$$

The magnetic field also gives rise to a Zeeman energy term $E_Z$, which can be written as

$$E_Z=-\frac{\hbar e}{m_0}\kappa B j_z. \tag{8}$$

Here $\kappa$ is another Luttinger parameter.[26]

### B. Choice of basis

The single-hole Hamiltonian is

$$H=H_L+V_\parallel(\rho)+V_\perp(z)+E_Z. \tag{9}$$

In the axial approximation the Hamiltonian $H$ is rotationally invariant around the $z$ axis. It therefore proves useful to introduce the *total* angular momentum $\mathbf{F}=\mathbf{J}+\mathbf{L}$, where **J** is the angular momentum of the band-edge Block function and **L** the envelope angular momentum. Since now $\mathbf{F}_z$ is a constant of the motion we can find simultaneous eigenstates of $H$ and $\mathbf{F}_z$. Labeling these states by $f_z$, where $\hbar f_z$ is the eigenvalue of $\mathbf{F}_z$, a general hole state can be written as

$$\psi_{f_z}(\mathbf{r})=\sum_{j_z} F^{j_z}(\rho,z)e^{i\phi(f_z-j_z)}\left|\tfrac{3}{2},j_z\right\rangle, \tag{10}$$

where $\left|\frac{3}{2},j_z\right\rangle$ is the band-edge Bloch function and $F(\rho,z)$ the envelope function.

The diagonal terms of $H$ are separated into an in-plane part and a $z$-dependent part, which describes a one-dimensional quantum-well problem. The in-plane problem is that of a two-dimensional (2D) harmonic oscillator in a mag-

TABLE I. Subband ($s$) and angular momentum states ($l$) that are coupled by the off-diagonal terms in the Kohn-Luttinger Hamiltonian. We only list the lowest subband state; all higher subband states with the same parity are also coupled.

| $S^+_{3/2}$ | | $S^+_{-3/2}$ | | $S^+_{1/2}$ | | $S^+_{-1/2}$ | | $S^-_{1/2}$ | | $S^-_{-1/2}$ | | $P^+_{5/2}$ | | $P^+_{-5/2}$ | |
|---|---|---|---|---|---|---|---|---|---|---|---|---|---|---|---|
| $s$ | $l$ | $s$ | $l$ | $s$ | $l$ | $s$ | $l$ | $s$ | $l$ | $s$ | $l$ | $s$ | $l$ | $s$ | $l$ |
| HH1 | 0 | HH2 | -3 | HH2 | -1 | HH1 | -2 | HH1 | -1 | HH2 | -2 | HH2 | 1 | HH1 | -4 |
| LH2 | 1 | LH1 | -2 | LH1 | 0 | LH2 | -1 | LH2 | 0 | LH1 | -1 | LH1 | 2 | LH2 | -3 |
| LH1 | 2 | LH2 | -1 | LH2 | 1 | LH1 | 0 | LH1 | 1 | LH2 | 0 | LH2 | 3 | LH1 | -2 |
| HH2 | 3 | HH1 | 0 | HH1 | 2 | HH2 | 1 | HH2 | 2 | HH1 | 1 | HH1 | 4 | HH2 | -1 |

netic field, and we use its solutions for the heavy-hole part as a basis for the in-plane part. These oscillator functions can be written as[27]

$$\Phi_{nl}(\rho,\phi)=C_{nl}(i\rho)^{|l|}e^{-\rho^2/2a^2}e^{il\phi}L_n^{|l|}(\rho^2/a^2). \quad (11)$$

Here $C_{nl}$ is a normalization constant (see Appendix A) and $L_n^l$ is a generalized Laguerre polynomial. The length $a$ is related to the magnetic length $a_c=(\hbar/eB)^{1/2}$ and the harmonic length $l_0=(\hbar/m_h\omega_0)^{1/2}$ by

$$a^2=2\frac{l_0^2a_c^2}{(l_0^4+4a_c^4)^{1/2}}. \quad (12)$$

The energy levels of the 2D oscillator are[27]

$$E_{nl}=(2n+|l|+1)\hbar\omega-\tfrac{1}{2}\hbar\omega_c l, \quad (13)$$

where $\omega=(\omega_0^2+\omega_c^2/4)^{1/2}$ and $\omega_c=eB/m_h$ is the cyclotron frequency in terms of the heavy-hole mass. In the limit $B\to 0$ we have that $a=l_0$ and $\omega=\omega_0$, so the wave functions (11) and the energy levels (13) reduce to the corresponding quantities in the field-free case.[24] With no parabolic confinement potential $a=\sqrt{2}a_c$. In this limit $E_{nl}=[n+(|l|-l)/2+1/2]\hbar\omega_c=(N+1/2)\hbar\omega_c$, where $N$ is the Landau-level index. So with no confinement potential the levels are *independent* of $l$ (for positive $l$).

As a convenient basis for the subband part we use simple trigonometric functions, viz.,

$$f_s(z)=\sqrt{2/W}\sin[s\pi(z+W/2)/W], \quad |z|\le W/2, \quad (14)$$

and zero otherwise. $W$ is allowed to be slightly larger than the width of the quantum well. These functions lead to simple integrals and avoid the use of continuum functions in the subband basis. This set, however, is not complete. But for large offsets the wave function decays rapidly inside the barrier material. The neglect of the wave-function tail for $|z|>W/2$ results therefore only in an exponentially small error. The optimum expansion width (for a fixed number of subbands in the basis) could be treated as a variational parameter. A good first estimate can be found by minimizing the energy for a single subband. To lowest order one then finds

$$W=w(1+2/V_{\rm Off}^{1/2}), \quad (15)$$

where $V_{\rm Off}=2mw^2\Delta E_v/\hbar^2$, $w$ is the actual quantum-well width, and $m$ is the effective mass of the subband in question.

In terms of the in-plane basis (11) and subband basis (14) the hole wave function is expanded as

$$\psi^{\pm}_{f_z}(\mathbf{r})=\sum_{j_z,n,s}C(n,s,j_z)\Phi_{n,f_z-j_z}(\rho,\phi)f_s(z)|\tfrac{3}{2},j_z\rangle \quad (16)$$

for states with even $(+)$ and odd $(-)$ parity and total angular momentum $f_z$. The energy is found variationally by minimizing with respect to the expansion coefficients $C(n,s,j_z)$. It is convenient to label the states in Eq. (16) in a spectroscopic manner. Usually the term with smallest $|l|$ is dominant, and we use it to label the expansion. Thus, states with an $l=0$ term and total angular momentum $f_z$ will be referred to as $S_{f_z}$, etc. The various terms that are coupled in the axial approximation have been listed in Table I.

In the present basis *all* matrix elements of the single-hole Hamiltonian can be found analytically. This is accomplished by using the operator relations in Appendix A for the off-diagonal terms in the Luttinger Hamiltonian. These relations are also used to calculate the matrix elements of the light-hole kinetic energy within the heavy-hole basis. Since we used a large number of heavy-hole basis functions, the low-lying light-hole states are adequately described in this basis.

With two holes in the dot interacting via a Coulomb potential we expand the two-hole wave function in terms of antisymmetrized single-hole product states. Since the Coulomb interaction is invariant with respect to simultaneous rotations of both holes the total (two-hole) angular momentum in the $z$ direction is still conserved. The Bloch part now contributes an angular momentum $J_z=j_z+j_z'$ so a state with total angular momentum $F_z$ has an envelope momentum $L_z=F_z-J_z$. Since $L_z=l_z+l_z'$, infinitely many single-hole envelopes enter into the expansion. But from Eq. (13) we see that the energy levels increase with $|l|$ so we keep the basis finite by only retaining terms with $|l|\le l_{\max}$. As the Coulomb potential is rotationally invariant it only couples states with the same $L_z$. Furthermore, it is diagonal in spin-space. In the actual calculation the Coulomb matrix elements are reduced to one-dimensional integrals that must be done numerically.[24]

## III. RESULTS AND DISCUSSION

This section contains the results from the numerical calculations. For the single-hole problem we use a standard diagonalization technique to compute the energy levels. This approach, however, is inadequate for the two-hole problem as it requires a large number of basis functions. Instead we

resort to the iterative relaxation technique used previously for the field-free case. It is both simple and capable of finding eigenvalues of large matrices efficiently. As shown in Ref. 24 it provides (in its simplest form) the ground-state energies for the different symmetries.

For the GaAs quantum dot we use the material parameters[28]

$$\gamma_1 = 6.85, \quad \gamma_2 = 2.1, \quad \gamma_3 = 2.9, \quad \kappa = 1.2, \tag{17}$$

and a static dielectric constant $\epsilon = 12.74\epsilon_0$. To ease the computational effort we also use these material parameters for the $Al_xGa_{1-x}As$ barrier material. This avoids the complicated matching of the hole wave function at the material interfaces. The justification of this simplification comes in two parts. First, the mismatch of the material parameters between the well and barrier materials is relatively small. But more importantly, we are by assumption in the situation of strong confinement in the growth direction. The contribution to the energy functional from the wave-function penetration into the barrier material is consequently subordinate. Having tailored our subband basis to this situation it is therefore consistent to ignore the mismatch between the material parameters.

The confinement in the growth direction is caused by the valence-band offset $\Delta E_v$. Assuming a 65/35 division of the band-gap difference $\Delta E_g(x) = 1247x$ between the conduction and valence bands, the offset follows from the relation $\Delta E_v = 0.35\Delta E_g(x) = 436x$ meV when $x < 0.45$. For alloys with $x = 0.3$ we thus have $\Delta E_v = 130$ meV. (The resulting in-plane dispersion relation for a 100-Å-wide quantum well is shown in Ref. 24.) For the 100-Å-thick quantum well that we will be studying, the lowest subband edges then occur at the following energies: HH1=7.18 meV, LH1=22.10 meV, HH2=28.46 meV, and HH3=62.81 meV.[29] Here HH*s* (LH *s*) refers to the *s*th heavy-hole (light-hole) subband edge.

In the absence of the magnetic field the single-hole levels are twofold Kramer's degenerate: States with $\pm f_z$ have the same energy. The magnetic field can lift this degeneracy. The energy fulfills now instead the time-reversal symmetry-relation

$$E_{f_z}(\mathbf{B}) = E_{-f_z}(-\mathbf{B}). \tag{18}$$

Very few experiments have been performed on hole states in quantum dots. As far as we know there have been no experiments on hole levels in GaAs quantum dots with parabolic confinement potentials. In the experiments by Ashoori *et al.*[2] on *electrons* in parabolic GaAs quantum dots a good agreement between experiment and a simple model of electrons in a parabolic potential was obtained. In particular the lowest-energy state was well described by a parabolic confinement potential with $\hbar\omega_0 = 5.4$. We tentatively use this value for the confinement potential acting on the holes, resulting in uncoupled heavy-hole and light-hole oscillator energies (in zero field) of 5.4 and 3.9 meV, respectively. We note that $\hbar\omega_0 = \hbar\omega_c$ for $B_c = 5.2$ T: For $B \gg B_c$ the magnetic-field confinement dominates the confinement potential, for $B \ll B_c$ the situation is reversed.

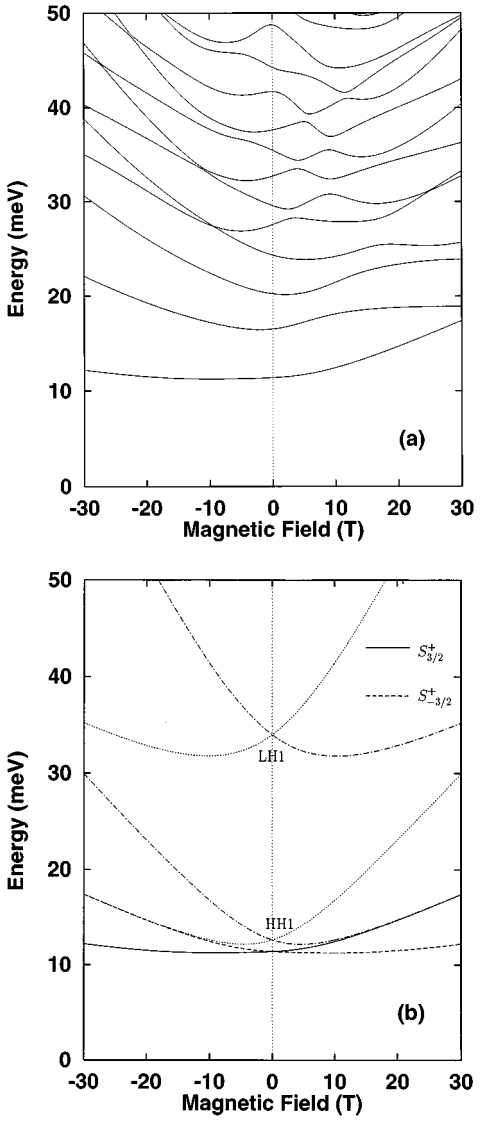


FIG. 1. Energy levels as a function of magnetic field. The quantum-well thickness is 100 Å and the valence-band offset $\Delta E_v = 130$ meV. The parabolic confinement potential is $\hbar\omega_0 = 5.4$ meV. (a) Energy levels of the symmetry state $S^+_{3/2}$. Note that no levels cross. (b) Energy levels of the lowest-lying $S^+_{3/2}$ (solid line) and $S^+_{-3/2}$ (dashed line) states. Also shown are the related uncoupled levels for HH1 ($l=0$) and LH1 ($l=\pm 2$) (dash-dotted lines for $f_z = 3/2$ and dotted lines for $f_z = -3/2$).

### A. Single-hole energies

In Fig. 1 we consider a parabolic quantum dot made from a 100-Å-thick $GaAs/Al_{0.3}Ga_{0.7}As$ [001] quantum well. Figure 1(a) displays the 14 lowest-energy levels of the $S^+_{3/2}$ state as a function of the magnetic field. As symmetry forbids the coupled levels to cross we see instead strong anticrossings of the levels. In Fig. 1(b) we show the lowest energy levels of the two states with $S^+_{3/2}$ and $S^+_{-3/2}$ symmetry, which are degenerate at $B=0$ and split at nonzero magnetic field. The symmetry relation (18) is evident from the figure. For comparison we have also included in Fig. 1(b) some related uncoupled levels (which are obtained with the off-diagonal terms in $H_L$ set to zero) corresponding to HH1 ($l=0$) and LH1 ($l=\pm 2$). We see that the inclusion of coupling due the

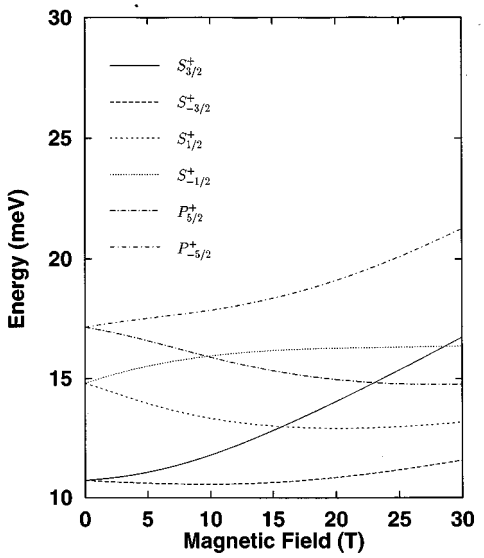


FIG. 2. The lowest-energy levels for the six different symmetries $S^+_{3/2}$, $S^+_{-3/2}$, $S^+_{1/2}$, $S^+_{-1/2}$, $P^+_{5/2}$, and $P^+_{-5/2}$. The quantum well is the same as in Fig. 1.

off-diagonal terms of $H_L$ lowers the energies of the two states, a fact that follows directly from the variational principle as these are the lowest-energy states of that particular symmetry. Furthermore, as levels of the same symmetry are forbidden to cross, they show in general a weaker field dependence compared to the uncoupled ones. From Fig. 1(b) we also notice that the level $S^+_{3/2}(S^+_{-3/2})$ is very close to the uncoupled HH1 level with $l=0$ for $B \gtrsim 10 (B \lesssim -10)$ T. As shown in Appendix B, this state approaches a Landau level that is completely decoupled in the strong-field limit.[30] Note that for $B>0$, the state $S^+_{3/2}$ is higher in energy than $S^+_{-3/2}$, while the opposite is true for the uncoupled levels, which are ordered according to their Zeeman terms. We shall discuss this behavior together with Figs. 2 and 3.

Figure 2 displays the lowest energy levels for the six different symmetries $S^+_{\pm 3/2}$, $S^+_{\pm 1/2}$, and $P^+_{\pm 5/2}$, all of which have even parity. The corresponding odd-parity symmetries are shown in Fig. 3. The relative importance of the different terms in the Hamiltonian can qualitatively be classified into three different regimes: a subband-dominated regime ($\Delta E_{\rm sub} \gg \hbar\omega_0, \hbar\omega_c$), a confinement-dominated regime ($\hbar\omega_0 \gg \Delta E_{\rm sub}, \hbar\omega_c$), and a Landau-regime ($\hbar\omega_c \gg \Delta E_{\rm sub}, \hbar\omega_0$). In the subband-dominated regime the off-diagonal terms in the Kohn-Luttinger Hamiltonian are less important and all states approach the subband minimum HH1. The ordering of the magnetic-field split levels is the same as in the uncoupled case; i.e., the state where the HH1 subband is associated with an in-plane envelope with the largest (and positive) $l$ is lowest in energy (see Table I). Thus $S^{\pm}_{\pm 1/2}(P^+_{5/2})$ will be lower in energy compared with $S^{\pm}_{\mp 1/2}(P^+_{-5/2})$. An exceptional case occurs for $S^+_{\pm 3/2}$ as then HH1 is coupled to an envelope with $l=0$. In this case the ordering is simply given by the Zeeman term, and $S^+_{3/2}$ is lower than $S^+_{-3/2}$ in the absence of couplings. With couplings, the ordering is inverted, and $S^+_{-3/2}$ becomes lower (mainly) due to strong coupling with the LH1 ($l=-2$) level.

In the confinement-dominated regime there is strong intersubband coupling and the dominant contribution to the energy comes from the envelope with the smallest angular momentum $|l|$. In the Landau regime the magnetic field is the dominant factor, and the levels approach a Landau-level structure (see Appendix B).

The present case ($\hbar\omega_0 = 5.4$ meV) is intermediate between the subband-dominated and confinement-dominated regimes, at least for small magnetic fields. The ordering of the single-hole levels follows the above analysis for the subband-dominated regime, with the exception of the $S^+_{\pm 3/2}$ states. The strong couplings induced by the confinement potentials and the magnetic field invert the ordering such that the $S^+_{-3/2}$ state is lower than $S^+_{3/2}$ for all values of the magnetic field. We have also examined the case with smaller values of $\hbar\omega_0$. For $0 < \hbar\omega_0 < 2.5$ meV the $S^+_{\pm 3/2}$ states cross at a finite magnetic field in addition to the crossing at the zero field. For $\hbar\omega_0 \simeq 2.5$ meV these two points of crossing confluence, and $S^+_{-3/2}$ becomes the ground state for all positive values of B.

For strong magnetic fields the states in Figs. 2 and 3 approach the corresponding Landau-level structure treated in Appendix B. Here we simply note the following: In the field-free case it was found that the ground state became primarily light-hole-like in the strong confinement limit. This was explained as a mass-induced crossover from quasi-2D to quasi-1D behavior. Even though the magnetic field also gives rise to a parabolic confinement potential, the strong-field limit is different. The wave functions in the Landau regime are mass independent. In this limit the ground state is degenerate and it can be chosen as either heavy-hole- or light-hole-like. There is consequently no mass-induced symmetry change of the ground state in the high-magnetic-field limit.

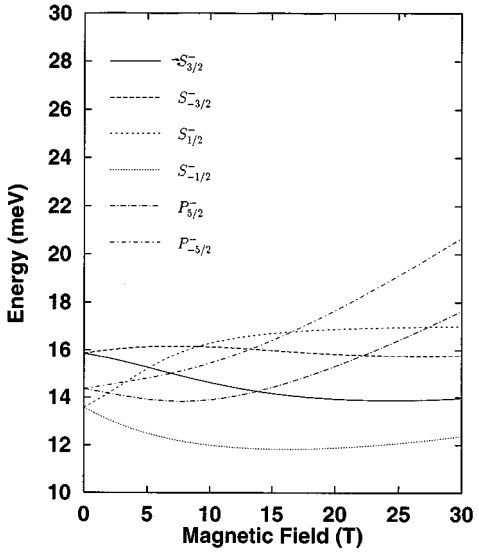


FIG. 3. Same as Fig. 2, but now for the lowest-energy levels of the odd-parity states $S^-_{3/2}$, $S^-_{-3/2}$, $S^-_{1/2}$, $S^-_{-1/2}$, $P^-_{5/2}$, and $P^-_{-5/2}$.

### B. Two-hole energies

We now add a second hole to the dot and calculate the resulting two-hole energies. The presence of both the Coulomb interaction and the off-diagonal terms in the Luttinger Hamiltonian necessitates the use of a large basis set. For

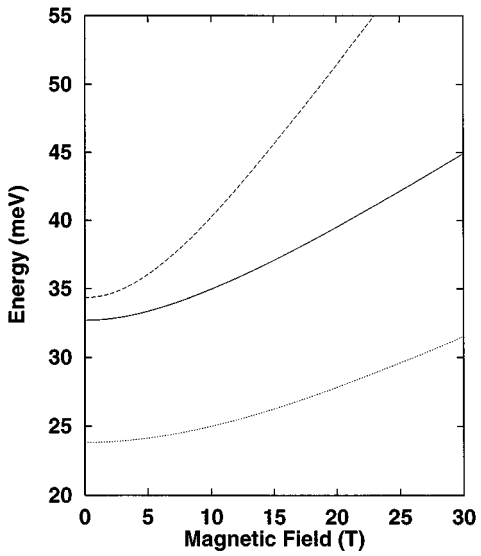


FIG. 4. The two-hole energy for the state $S_0^+$ as a function of the magnetic field (solid line). The quantum-well thickness is 100 Å and the valence-band offset $\Delta E_v = 130$ meV. The dashed line is obtained ignoring all off-diagonal terms in the Luttinger Hamiltonian, hence using a one-band model. The dotted line is the energy of two noninteracting holes (including the off-diagonal couplings in the Luttinger Hamiltonian). The Coulomb interaction raises the energy by 8.88 meV at $B=0$ and 13.37 meV at $B=30$ T.

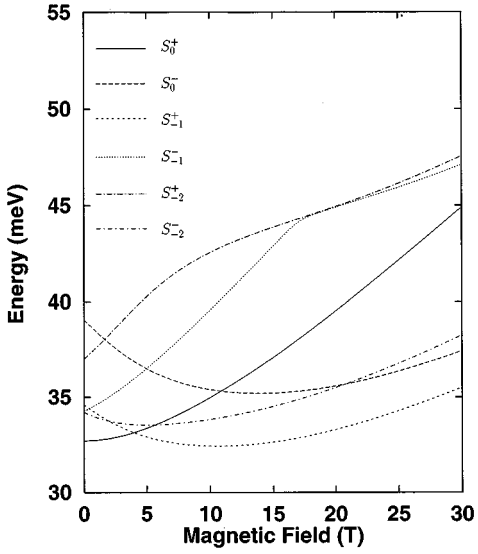


FIG. 5. The lowest two-hole energies for the states $S_0^{\pm}$, $S_{-1}^{\pm}$, and $S_{-2}^{\pm}$. The quantum well is the same as in Fig. 4. The ground state in zero field is $S_0^+$. It crosses the state $S_{-1}^+$ at $B \simeq 3.95$ T as explained in the text.

each hole we consequently include the four lowest subbands with the correct parity. In the lateral direction we use the 28 lowest oscillator states, corresponding to different angular momentum states with $l=0,\pm1,\pm2,\pm3$. This gives a total basis of 23 552 functions, half of which have even and odd parity. The large number of angular states included in the basis is essential in order to model important correlations between the holes as well as to obtain an accurate description of the single-hole states. Using the relaxation method (as described in Ref. 24) we can efficiently obtain the energy of the lowest-lying level for each specified symmetry, even with such a large basis.

We consider the same quantum well as before, which had a thickness of 100 Å. The expansion width $W$ for the subband basis remains to be determined. The estimate (15), based on a single subband, gives $W=117$ Å. As we include four subbands the optimum expansion width (used in the calculation) is found to be $W=165$ Å.

In Fig. 4 the two-hole state $S_0^+$ is shown (solid line) as a function of the magnetic field. We know that this is the ground state in zero field,[24] and expect it to be the ground state also in the presence of the magnetic field, at least in the weak-field limit. To assess the importance of the Coulomb interaction and the off-diagonal terms in the Luttinger Hamiltonian we have also included in Fig. 4 the two-hole energy without these effects. The dotted line is the energy of two noninteracting holes, while the dashed line is the two-hole energy neglecting the coupling terms in the Luttinger Hamiltonian (a one-band model).[31] The energy of the one-band model is substantially higher, which is not surprising in light of Fig. 1(b). There we saw the importance of the off-diagonal coupling terms in the Luttinger Hamiltonian, but the inclusion of the Coulomb interaction is also essential as it raises the energy due to the mutual repulsion between the two holes. As expected both these effects become more prominent as the magnetic field increases.

To further elucidate the importance of the Coulomb interaction on the two-hole states we present in Figure 5 the lowest two-hole states belonging to different symmetries. We notice that the $S_0^+$ state is indeed the ground state for small magnetic fields, but it gives place to $S_{-1}^+$ at $B \simeq 3.95$ T. As a simple step in understanding Fig. 5 we have listed in Table II the dominant single-hole products that build up the two-hole states. Based on these dominant single-hole products we can qualitatively understand the ordering of the two-hole levels of Fig. 5.

For sufficiently weak magnetic fields the $S_{\pm 3/2}^+$ levels are the lowest single-hole states (see Figs. 2 and 3). The two-hole ground state should in this limit thus consist primarily of the product state $S_{3/2}^+ S_{-3/2}^+$, which belongs to the $S_0^+$ state. (The other two-hole states $S_{\pm 3}^+$ lie higher in energy due to the Pauli exclusion principle.) With increasing magnetic fields we see from Figs. 2 and 3 that the ordering of the single-hole levels is changed. While $S_{-3/2}^+$ remains the lowest single-hole state at all magnetic fields, state $S_{3/2}^+$ crosses $S_{-1/2}^-$ at $B \simeq 11$ T and $S_{1/2}^+$ at $B \simeq 16$ T (see Fig. 2). It is therefore not surprising that $S_0^+$ ceases to be the ground state at higher magnetic fields. However, to fully understand the ordering of the two-hole states in Fig. 5 we must also take into account the effect of the Coulomb interaction: Neglecting this effect one would erroneously conclude that $S_{-2}^-$ would be the ground state for 11 T $\lesssim B \lesssim$ 16 T. From Table II we see that the dominant single-hole product states for moderate magnetic fields are $S_{3/2}^+ S_{-3/2}^+$ for $S_0^+$, $S_{1/2}^+ S_{-3/2}^+$ for $S_{-1}^+$, and $S_{-1/2}^- S_{-3/2}^+$ for $S_{-2}^-$, which differ only in the first single-hole factor. The angular momentum dependence of the different single-hole states are shown in Table I. The dominant contribution comes from the angular momentum state associated with the HH1 subband, which are $l=0$ for $S_{3/2}^+$, $l=1$ for $S_{-1/2}^-$, and

TABLE II. The dominant single-hole product states that couple to form the two-hole states in Fig. 5. Only the contributions from the $S$-like (i.e., $l=0$) single-hole envelopes are listed.

| $S_0^+$ | $S_0^-$ | $S_{-1}^+$ | $S_{-1}^-$ | $S_{-2}^+$ | $S_{-2}^-$ |
|---|---|---|---|---|---|
| $S_{3/2}^+S_{-3/2}^+$ | $S_{3/2}^+S_{-3/2}^-$ | $S_{-3/2}^+S_{1/2}^+$ | $S_{-3/2}^+S_{1/2}^-$ | $S_{-3/2}^+S_{-1/2}^+$ | $S_{-3/2}^+S_{-1/2}^-$ |
| $S_{3/2}^-S_{-3/2}^-$ | $S_{3/2}^-S_{-3/2}^+$ | $S_{-3/2}^-S_{1/2}^-$ | $S_{-3/2}^-S_{1/2}^+$ | $S_{-3/2}^-S_{-1/2}^-$ | $S_{-3/2}^-S_{-1/2}^+$ |
| $S_{1/2}^+S_{-1/2}^+$ | $S_{1/2}^+S_{-1/2}^-$ | $S_{-1/2}^+S_{-1/2}^+$ | $S_{-1/2}^+S_{-1/2}^-$ | $S_{-1/2}^+S_{-3/2}^+$ | $S_{-1/2}^+S_{-3/2}^-$ |
| $S_{1/2}^-S_{-1/2}^-$ | $S_{1/2}^-S_{-1/2}^+$ | $S_{-1/2}^-S_{-1/2}^-$ | $S_{-1/2}^-S_{-1/2}^+$ | $S_{-1/2}^-S_{-3/2}^-$ | $S_{-1/2}^-S_{-3/2}^+$ |

$l=2$ for $S_{1/2}^+$. With increasing magnetic fields the holes are squeezed closer together, and it becomes energetically favorable to have one of the holes enter a higher angular momentum state in order to minimize the Coulomb repulsion. This effect is greater for the $S_{-1}^+$ state compared with $S_{-2}^-$, so it becomes the two-hole ground state for a sufficiently strong magnetic field.

The inclusion of the Coulomb interaction is therefore essential for an understanding of the two-hole spectra.

## IV. SUMMARY

We have calculated the single-hole and two-hole states of a parabolic quantum dot in the presence of a perpendicular magnetic field. The inclusion of the off-diagonal terms in the Luttinger Hamiltonian is shown to be important, leading to anticrossings of the single-hole levels and in general a weaker field dependence. The Coulomb interaction between the holes leads to strong correlation effects. As the applied magnetic field is increased the total angular momentum of the ground state changes in order for the holes to minimize their total energy.

Both the valence-band mixing and the effect of the Coulomb interaction increase as the magnetic field is increased. As far as the quantum-well width is concerned, the dots considered experimentally in Ref. 1 were slightly wider (150 – 200 Å) than the ones treated here. In wider dots the Coulomb energies decrease, but the valence-band mixing and correlation effects become even more important.

In the field-free case of Ref. 24 it was found that the symmetry of the single-hole and two-hole states changed from primarily heavy-hole-like to primarily light-hole-like for sufficiently strong parabolic confinement potential. In the high-field limit there is no such symmetry change induced by the magnetic field.

## ACKNOWLEDGMENTS

One of us (F.B.P.) is grateful to Norges Forskningsråd for financial support during his stay at the University of Illinois. He would also like to thank Y.-C. Chang's group for their hospitality during his visit. The authors acknowledge the use of computing facilities provided by the University of Illinois, Materials Research Laboratory under Contract No. NSF/DMR-89-20538, as well as the use of the CRAY Y-MP4D/464 at the University of Trondheim.

## APPENDIX A: OPERATOR RELATIONS FOR THE 2D HARMONIC OSCILLATOR IN A MAGNETIC FIELD

In this appendix we generalize the operator relations for $k_\pm = k_x \pm ik_y$ for the field-free case considered in Ref. 24. In cylindrical coordinates these operators take the form

$$k_\pm = -ie^{\pm i\phi}\left(\frac{\partial}{\partial r} \pm \frac{i}{r}\frac{\partial}{\partial \phi} \pm \frac{r}{2a_c^2}\right) \tag{A1}$$

in the presence of a magnetic field. The wave functions $|n,l\rangle$ can be written as

$$\Phi_{nl}(\rho,\phi) = C_{nl}(i\rho)^{|l|}e^{-\rho^2/2a^2}e^{il\phi}L_n^{|l|}(\rho^2/a^2), \tag{A2}$$

with the normalization constant

$$C_{nl} = \sqrt{\frac{n!}{\pi(n+|l|)!}}\left(\frac{1}{a}\right)^{|l|+1}. \tag{A3}$$

The phase in Eq. (A2) is chosen so as to simplify the operator relations. The length $a$ is related to the magnetic length $a_c$ and oscillator length $l_0$ by Eq. (12) in the text.

It proves useful to introduce the dimensionless quantity $\Lambda$ by

$$\Lambda = 2\left(\frac{a_c}{a}\right)^2. \tag{A4}$$

Using the properties of the Laguerre polynomial we find the following relations for $l>0$:

$$a_c k_+|n,l\rangle = \frac{1}{\sqrt{2}}(\Lambda^{1/2}+\Lambda^{-1/2})\sqrt{n}|n-1,l+1\rangle + \frac{1}{\sqrt{2}}(\Lambda^{1/2}-\Lambda^{-1/2})\sqrt{n+l+1}|n,l+1\rangle, \tag{A5}$$

$$a_c k_-|n,l\rangle = \frac{1}{\sqrt{2}}(\Lambda^{1/2}+\Lambda^{-1/2})\sqrt{n+1}|n+1,l-1\rangle + \frac{1}{\sqrt{2}}(\Lambda^{1/2}-\Lambda^{-1/2})\sqrt{n+l}|n,l-1\rangle, \tag{A6}$$

and when $l<0$

$$a_c k_+|n,l\rangle = \frac{1}{\sqrt{2}}(\Lambda^{1/2}+\Lambda^{-1/2})\sqrt{n-l}|n,l+1\rangle + \frac{1}{\sqrt{2}}(\Lambda^{1/2}-\Lambda^{-1/2})\sqrt{n+1}|n+1,l+1\rangle, \tag{A7}$$

$$a_c k_- |n,l\rangle = \frac{1}{\sqrt{2}}(\Lambda^{1/2}+\Lambda^{-1/2})\sqrt{n-l+1}\,|n,l-1\rangle + \frac{1}{\sqrt{2}}(\Lambda^{1/2}-\Lambda^{-1/2})\sqrt{n}\,|n-1,l-1\rangle, \tag{A8}$$

and finally for $l=0$:

$$a_c k_+ |n,0\rangle = \frac{1}{\sqrt{2}}(\Lambda^{1/2}+\Lambda^{-1/2})\sqrt{n}\,|n-1,1\rangle + \frac{1}{\sqrt{2}}(\Lambda^{1/2}-\Lambda^{-1/2})\sqrt{n+1}\,|n,1\rangle, \tag{A9}$$

$$a_c k_- |n,0\rangle = \frac{1}{\sqrt{2}}(\Lambda^{1/2}+\Lambda^{-1/2})\sqrt{n+1}\,|n,-1\rangle + \frac{1}{\sqrt{2}}(\Lambda^{1/2}-\Lambda^{-1/2})\sqrt{n}\,|n-1,-1\rangle. \tag{A10}$$

From these relations follows the effect of the off-diagonal terms in the Luttinger Hamiltonian on the basis functions. In the field-free case both $\Lambda$ and $a_c$ diverge such that $\Lambda/a_c^2 = 2/l_0^2$. The relations (A5)–(A10) then reduce to those of Ref. 24. With no parabolic confinement potential $\Lambda = 1$ and we recover the relations used in the Landau-level treatment of magneto-excitons.[32]

The light-hole diagonal elements can be related to the heavy-hole part by

$$H_l^{\parallel} = H_h^{\parallel} - \frac{\hbar^2}{m_0}\gamma_2(k_x^2+k_y^2), \tag{A11}$$

where $H^{\parallel}$ refers to the in-plane part only. With the magnetic field present we have that

$$k_x^2+k_y^2 = k_+k_- - i[k_x,k_y] = k_+k_- - 1/a_c^2. \tag{A12}$$

The matrix elements of the light-hole kinetic energy within the heavy-hole basis then follow immediately combining (A12) with (A5)–(A10).

## APPENDIX B: LANDAU-LEVEL LIMIT OF THE 2D OSCILLATOR

In Ref. 24 the field-free problem was addressed. In this Appendix we consider the opposite limit, viz., no parabolic confinement potential. It is then convenient to use the Landau gauge $\mathbf{A} = B(-y,0,0)$. All discussions given here only apply for $B>0$. For $B<0$, we can use the time-reversal relation (18) to deal with states with opposite angular momemtum. The motion in the $x$ direction is now just plane waves, while the $y$ direction corresponds to a 1D harmonic oscillator. Representing the magnetic field in terms of the raising and lowering operators for the 1D oscillator the Landau eigenfunctions are easily found to be of the form

$$\Psi = \begin{bmatrix} c_1 f_1(z)\Phi_N(y) \\ c_2 f_2(z)\Phi_{N-1}(y) \\ c_3 f_3(z)\Phi_{N-2}(y) \\ c_4 f_4(z)\Phi_{N-3}(y) \end{bmatrix}, \tag{B1}$$

where $f_i$ are subband functions, $c_i$ are constants, and $\Phi_N$ 1D harmonic oscillator functions. We have here only included the lowest subband function in each product as this is the dominant contribution. For the solution (B1) to be valid we need to take $c_i \equiv 0$ in the products $c_i f_i(z)\Phi_N(y)$ whenever $N<0$. It then follows immediately that for $N=0$, we must put $c_2 = c_3 = c_4 = 0$, and we have a completely decoupled Landau level as a solution.

The Landau solutions (B1) and in particular the uncoupled level should also be found as the asymptotic limit of our solutions for high magnetic fields. In this limit the operator relations (A5)–(A10) reduce to

$$\begin{aligned} a_c k_+ |n,l\rangle &= \sqrt{2}\sqrt{n}\,|n-1,l+1\rangle, \quad l\geqslant 0, \\ a_c k_- |n,l\rangle &= \sqrt{2}\sqrt{n+1}\,|n+1,l-1\rangle, \quad l>0, \\ a_c k_+ |n,l\rangle &= \sqrt{2}\sqrt{n-l}\,|n,l+1\rangle, \quad l<0, \\ a_c k_- |n,l\rangle &= \sqrt{2}\sqrt{n-l+1}\,|n,l-1\rangle, \quad l\leqslant 0, \end{aligned} \tag{B2}$$

while the corresponding energy levels now become

$$E = \left(n + \frac{|l|-l}{2} + \frac{1}{2}\right)\hbar\omega_c = (N+\tfrac{1}{2})\hbar\omega_c, \tag{B3}$$

where $N$ is the Landau-level index used in Eq. (B1);

$$N = \begin{cases} n, & l\geqslant 0 \\ n-l, & l\leqslant 0. \end{cases} \tag{B4}$$

A general solution based on the spherical oscillators can then be written as

$$\Psi = \begin{bmatrix} c_1 f_1(z)|n_1,l\rangle \\ c_2 f_2(z)|n_2,l+1\rangle \\ c_3 f_3(z)|n_3,l+2\rangle \\ c_4 f_4(z)|n_4,l+3\rangle \end{bmatrix} \tag{B5}$$

since the operator relations (B2) now only couple *two* oscillator levels.

The simplest cases to consider are those where $l\geqslant 0$ or $l\leqslant -3$. For $l\geqslant 0$ it follows from Eqs. (B1) and (B5) that $n_1 = N$, $n_2 = N-1$, $n_3 = N-2$, and $n_4 = N-3$ and we must take $c_i = 0$ whenever $n_i < 0$. For $l\leqslant -3$, $n_1 = n_2 = n_3 = n_4 = N+l$. The relations between $n$, $l$ and $N$ for intermediate $l$ values follow from the operator relations (B2).

It is now clear that uncoupled levels in the spherical-oscillator formulation only occur for $l\geqslant 0$ and $n_1 = 0$, corresponding to $N=0$. This is to be coupled to the lowest subband state to give the uncoupled level. Thus, in the high

magnetic-field limit the levels with symmetries $L^{(-)^L}_{L+3/2}$ (e.g., $S^+_{3/2}, P^-_{5/2}, D^+_{7/2}, \ldots$) approaches the corresponding uncoupled level. However, it is important to keep in mind that for these symmetries the coupled levels will in general be lower in energy compared to the uncoupled ones.

From the above analysis we can also deduce the degeneracy in the high-field limit. Since the Landau-level index $N$ is independent of $l$ for positive $l$ we have that all the states $L^{(-)^L}_{L+3/2}, (L=0,1,2,3, \ldots)$ will approach the same energy in the high-field limit.


[1] R.C. Ashoori, H. L. Stormer, J. S. Weiner, L. N. Pfeiffer, S. J. Pearton, K. W. Baldwin, and K. W. West, Phys. Rev. Lett. **68**, 3088 (1992).

[2] R.C. Ashoori, H. L. Stormer, J. S. Weiner, L. N. Pfeiffer, K. W. Baldwin, and K. W. West, Phys. Rev. Lett. **71**, 613 (1993).

[3] Ch. Sikorski and U. Merkt, Phys. Rev. Lett. **62**, 2164 (1989).

[4] A. Kumar, S. E. Laux, and F. Stern, Phys. Rev. B **42**, 5166 (1990).

[5] P. Hawrylak, Phys. Rev. Lett. **71**, 3347 (1993).

[6] U. Merkt, J. Huser, and M. Wagner, Phys. Rev. B **43**, 7320 (1991).

[7] M. Wagner, U. Merkt, and A. V. Chaplik, Phys. Rev. B **45**, 1951 (1992).

[8] P. A. Maksym and T. Chakraborty, Phys. Rev. Lett. **65**, 108 (1990).

[9] M. Taut, Phys. Rev. A **48**, 3561 (1993).

[10] N. F. Johnson and M. C. Payne, Phys. Rev. Lett. **67**, 1157 (1991); Phys. Rev. B **45**, 3819 (1992).

[11] N. F. Johnson and L. Quiroga, Phys. Rev. Lett. **74**, 4277 (1995).

[12] G. W. Bryant, Phys. Rev. Lett. **59**, 1140 (1987).

[13] M. El-Said, J. Phys. I (France) **5**, 1027 (1995).

[14] D. Pfannkuche and R. R. Gerhardts, Phys. Rev. B **44**, 13 132 (1991).

[15] V. Gudmundsson and R. R. Gerhardts, Phys. Rev. B **43**, 12 098 (1991).

[16] R. Ugajin, Phys. Rev. B **51**, 10 714 (1995).

[17] W. Kohn, Phys. Rev. **123**, 1242 (1961).

[18] L. Brey, N. F. Johnson, and B. I. Halpern, Phys. Rev. B **40**, 10 647 (1989).

[19] F. M. Peeters, Phys. Rev. B **42**, 1486 (1990).

[20] P. Bakshi, D. A. Broido, and K. Kempa, Phys. Rev. B **42**, 7416 (1990).

[21] D. A. Broido and L. J. Sham, Phys. Rev. B **31**, 888 (1985).

[22] D. A. Broido, A. Cros, and U. Rössler, Phys. Rev. B **45**, 11 395 (1992).

[23] T. Darnhofer, D. A. Broido, and U. Rössler, Phys. Rev. B **50**, 15 412 (1994).

[24] F. B. Pedersen and Y.-C. Chang, Phys. Rev. B **53**, 1507 (1996).

[25] J. M. Luttinger, Phys. Rev. **102**, 1030 (1956).

[26] See Ref. 25. The small Zeeman term, proportional to the Luttinger parameter $q$ is dropped as it has a negligible effect.

[27] V. Fock, Z. Phys. **47**, 446 (1928).

[28] *Semiconductors. Physics of Group IV Elements and III-V Compounds*, edited by K. -H. Hellwege and O. Madelung, Landolt-Börnstein, New Series, Group III, Vol. 17, Pt. a (Springer, Berlin, 1982); *Semiconductors. Intrinsic Properties of Group IV Elements and III-V, II-VI, and I-VII Compounds*, edited by K. -H. Hellwege and O. Madelung, Landolt-Börnstein, New Series, Group III, Vol.22, Pt. a (Springer, Berlin, 1987).

[29] The subband energies used here differ slightly from those used in Ref. 24, as the latter were calculated with lower precision. However, the precise values of the subband energies are not crucial for any of the conclusions reached in this paper or in Ref. 24.

[30] Note, however, that since the uncoupled Landau levels have a stronger field dependence than the coupled ones, they will tend to cross the coupled levels. Thus, the *nearly* uncoupled levels will anticross very abruptly, and the uncoupled Landau levels will be traced out by different excited states of the nearly uncoupled levels.

[31] The two-hole states contain envelopes with different angular momentum $L$. For the one-band model we use the state with $L=0$ as this is the lowest state for small magnetic fields.

[32] M. Altarelli and N. O. Lipari, Phys. Rev. B **9**, 1733 (1974); G. J. Rees, J. Phys. C **4**, 2822 (1971).